17th World Conference on Earthquake Engineering, 17WCEE
Sendai, Japan - September 13th to 18th 2020

3D EFFECTIVE STRESS ANALYSIS METHOD AND ITS APPLICATION TO VARIOUS SOIL CONDITIONS IN LIQUEFIABLE GROUND

K. Ito [1], T. Sasaki [1], S. Higuchi [1], Y. Yamakawa [2]

[1] *Obayashi Corporation, ito.koji.ro@obayashi.co.jp, sasaki.tomohiro@obayashi.co.jp, higuchi.shunichi@obayashi.co.jp*
[2] *Tohoku University, yuki.yamakawa.c7@tohoku.ac.jp*

Abstract

This paper describes the numerical procedure of solving liquefiable ground problems and its verification and application based on a three-dimensional effective stress analysis method incorporating cyclic elasto-plastic constitutive model of soil. The following conclusions were drawn from the study: (1) The developed model was extended and confirmed to reproduce the behavior for various ranges of soil density. (2) The applicability of the procedure considering the material non-linearity of both the soil and RC structure was verified, simulating the centrifuge model test of a RC pile foundation in liquefiable ground with a similitude of 1/25. (3) The seismic effectiveness of lattice-type cement-treated soil improvement adjacent to an underground RC structure was confirmed based on the response results of the structure and soil improvement body. Moreover, rational and acceptable specifications of cement-treated soil improvement were presented.

Keywords: Liquefaction; Numerical simulation; RC underground structure; Centrifuge; Soil improvement

1. Introduction

In the seismic performance evaluation of underground reinforced concrete (hereinafter referred to as RC) structures, it is necessary to grasp the nonlinear response characteristics of the soil-structure interaction system. In addition, on the seismic reinforcement of underground structures installed a soil improvement body in which cement is mixed with the original ground on both sides of the structure (hereinafter referred to as the "cement-treated soil improvement"), it is necessary to consider the nonlinear response characteristics of the cement-treated soil improvement body same as the surrounding ground. With the increase in the level of design input seismic motion, the use of ground deformation and structural deformation that allows structural damage as an index for seismic performance evaluation leads to a performance-oriented design. The finite element method considering all in one the soil-structure interaction system is expected as a powerful tool for seismic design.

To apply a seismic reinforcement such as cement-treated soil improvement method, adoption of the seismic analysis including non-linear effects of the surrounding ground, the RC structures and the cement-treated soil improvement body entirely is desirable. For example, in the case of seismic reinforcement of underground structures with a block-type cement-treated soil improvement (an overall improvement pattern by overlapping and integrating cylindrical solid bodies) installed on both sides, the reinforcement effect has been studied based on the lateral loading test and its pushover analysis [1]. Similarly, a countermeasure against liquefaction, utilizing a lattice-type cement-treated soil improvement (an improved pattern in which cylindrical solid bodies are overlapped in a lattice type, such as the "TOFT"), as an economical block-type cement-treated soil improvement method [2], is used. In this case, seismic performance is mainly evaluated using a two-dimensional analysis in which the soil improvement body is replaced with the outer and inner walls, and the unimproved ground inside the lattice and the liquefiable ground are simplified with plane

strain condition. On the other hand, in nonlinear seismic response using a three-dimensional analysis that precisely reproduce the shape of the actual ground, structures and cement-treated soil improvement, there are few examples in which the analysis accuracy has been verified by comparison with experimental test results [3], [4]. In non-linear seismic response analysis including RC structures and cement-treated soil improvement body in the liquefiable ground, an effective stress analysis method incorporating a constitutive model of soil is required adequately expressing the process of pore-water pressure generation, accumulation and dissipation during and post-earthquake.

In this study, we first show the expansion and applicability of the constitutive model of soil used for liquefiable ground and cement-treated soil improvement body that reproduce the strength and deformation characteristics of materials with a wide range of soil density from loose saturated sand to dense saturated sand. Next, a three-dimensional effective stress analysis method was developed incorporating the expanded constitutive model of soil. From the comparison between the existing centrifuge model test results of RC pile foundation in liquefiable ground and its reproduction analysis, its applicability to the nonlinear coupled the soil-structure behavior was verified. Finally, assuming the countermeasure against liquefaction with a lattice-type cement-treated soil improvement for the underground RC structure in the liquefiable ground, a three-dimensional effective stress analysis was performed, and rational specifications of soil improvement were presented based on the response of the structure and cement-treated soil improvement body.

2. Constitutive model of soil and cement-treated soil improvement body

2.1 Subloading surface model

A subloading surface model (Hashiguchi et al.) was introduced as a constitutive model of soil and cement-treated soil improvement body. This model is an elasto-plastic constitutive equation for soil based on the concept of the rotational hardening and the subloading surface with tensile yield strength expressing cyclic plasticity [5] - [7]. Fig. 1 shows the relationship between the normal-yield surface and the subloading surface of on the *p*-*q* plane (*p*: mean effective stress, *q*: deviator stress, *F*: the normal-yield surface, *f*: the subloading surface, *H*: the isotropic hardening variable and β: the anisotropic variable). The subloading surface used in this study has a similar center fixed at the origin, a similar shape to the normal-yield surface through the current stress point σ and a normal-yield subloading surface size ratio *R* (the size of the subloading surface relative to the normal-yield surface). In this study, we introduced the tensile strength ratio ξ (ξ=0 for the soil and $\xi \neq 0$ for the cement-treated soil improvement body) so that the behavior of the cement-treated soil improvement with tensile yield strength can be expressed in the same framework as soil.

2.2 Extension of subloading surface model

In this study, in the evolution law of the normal-yield subloading surface size ratio *R* that defines the plastic strain increment, *U(R)* is reduced associated with the cumulative plastic deviatoric strain ε_p^* as shown in Eqs. (1) and (2). Consequently, the occurrence of shear strain is reproduced that rapidly increased to a few percent can be obtained as that of undrained cyclic shear behavior observed in loose saturated sand [8].

$$\dot{R} = U(R)\|\dot{\varepsilon}^p\|\,, \quad \dot{\varepsilon}^p = D^p \tag{1}$$

$$U(R) = -\frac{u}{\exp(\zeta_1 \cdot \varepsilon^{p*})}\ln R\,, \qquad \varepsilon^{p*} = \int \|D^{p*}\|\,dt \tag{2}$$

Here, D^p is the plastic strain rate, D_p^* is the plastic deviatoric strain rate, *u* is a constant that defines the increment of plastic strain, and ζ_1 is a constant that defines the effect of plastic deviatoric strain. In isotropic hardening/softening due to shear, D_s^p in Eq. (3) reduces the same as in Eq. (2) with cumulative plastic deviatoric strain ε_p^* and adjusts the degree of isotropic hardening/softening due to shear. Thus, the generation of shear strain is reproduced so that the gradual increase to about several percent as that of observed in undrained cyclic shear behavior of dense saturated sand.

$$D_s^p = \mu\|D^{p*}\|\left(\frac{\|\sigma^*\|}{p} - m_d\right)\exp(\zeta_2 \cdot \varepsilon^{p*}) \tag{3}$$

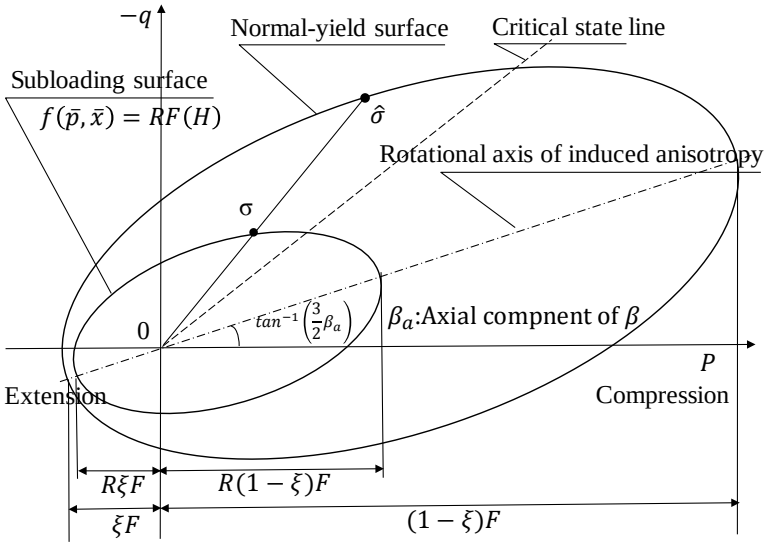

Fig. 1 Normal-yield surface and subloading surface in *p*-*q* plane

Table 1 Mechanical properties

Material	Silica sand No. 7 (D_r=60%)	
Compressional index	ρ, $\lambda/(1+e_0)$	0.00211
Swelling index	γ, $\kappa/(1+e_0)$	0.00047
Internal frictional angle	ϕ	33°
Initial normal-yield surface	F_0	100kN/m^2
Poisson's ratio	ν	0.33
Limit surface of rotatinal hardening	ϕ_b	33°
Evolution of rotatinal hardening	b_r	100
Evolution of normal-yield subloading surface size ratio R	u	5000
	ζ_1	1000
Isotropic hardening/softening due to shear*	μ	0.1
	ϕ_d	26.6°
	ζ_2	−10
Reference effective mean stress	$\sigma'_{m,ref}$	100kN/m^2
Elastic modulus at reference effective mean stress	E_{ref}	218647kN/m^2

* Isotropic hardening/softening due to shear is not available at μ=0.

Here, σ^* is the deviatoric stress, D_s^p is the plastic volume strain rate of isotropic hardening/softening due to shear, μ and m_d (function of ϕ_d) are the material constant of isotropic hardening/softening due to shear. ζ_2 is a material constant that regulates the effect of plastic deviatoric strain due to isotropic hardening/softening due to shear, and the behavior of loose, medium to dense sand is reproduced by $-\infty < \zeta_2 < 0$.
Table 1 shows the mechanical properties of the subloading surface model of silica sand No. 7 (D_r=60%). In the subloading surface model, the Modified cam-clay model is applied to the normal-yield surface, so the mechanical properties inherent to the subloading surface model consist of 7 parameters as, (a) Limit surface of rotational hardening ϕ_b, (b) Evolution of rotational hardening b_r, (c), (d) Evolution of normal-yield subloading surface size ratio u and ζ_1, and (e), (f), (g) Isotropic hardening/softening due to shear μ, ϕ_d, ζ_2. The main mechanical properties are set to be based on the physical and mechanical constants obtained in the material test of silica sand No. 7 (D_r=60%), and other constants are set to be on a trial.

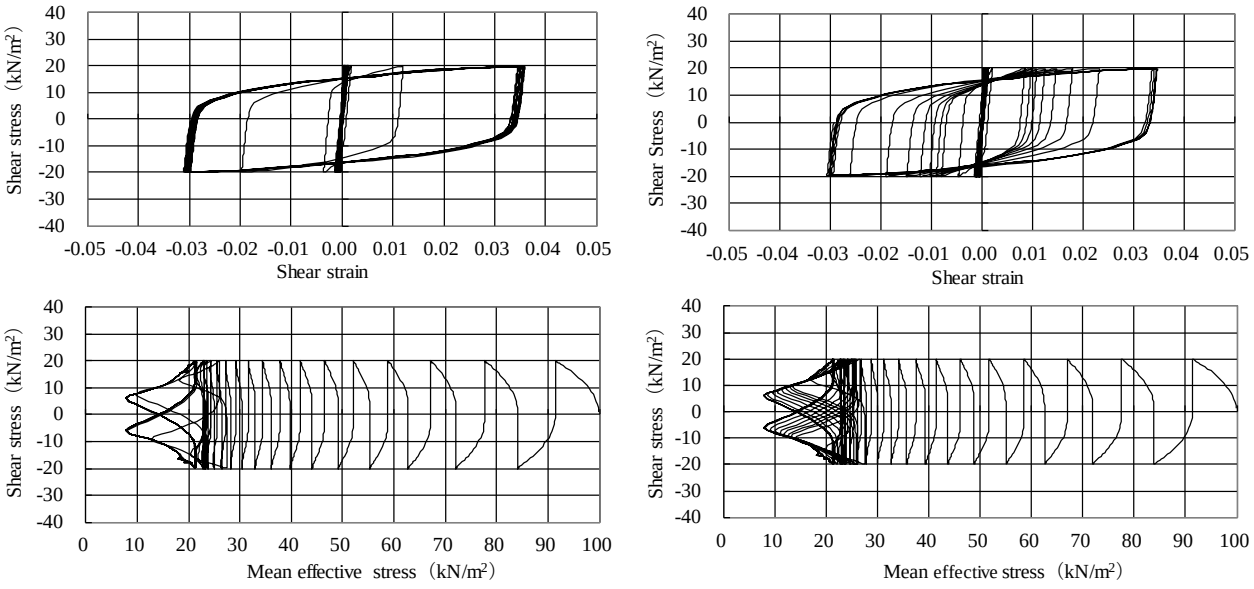

(Isotropic hardening/softening due to shear is not available) (Isotropic hardening/softening due to shear is available)

Fig. 2 Computed results of saturated sand behavior under undrained cyclic simple shear condition

2.3 Simulation of saturated sand behavior under undrained cyclic shear condition

Fig. 2 shows the simulation results obtained under undrained cyclic simple shear condition (shear stress ratio of 0.2), coefficient of earth pressure at rest K_0=1.0, initial mean effective stress σ_0'=100kN/m^2, in case of concerning the isotropic hardening/softening due to shear in Table 1 for loose and dense sand. In case of the loose sand, parameter μ is set as 0 for neglecting the isotropic hardening/softening due to shear. In the case of loose saturated sand, the effective stress path in the vicinity of the failure shows rapid approach to the origin and the shear strain increases rapidly. In the case of dense saturated sand, the effective stress path in the vicinity of the failure gradually approaches to the origin and the shear strain increases gradually. These tendencies are similar to the behavior of saturated sand with various density observed in the material test.

3. 3D effective stress analysis method

3.1 Overview of centrifuge model test results for verification

A centrifuge model test was conducted [9], [10] in order to obtain the verification data for the 3D effective stress analysis method considering the material nonlinearity of the structure and the liquefiable ground, to investigate the response characteristics of the RC pile foundation to the nonlinear range in the liquefiable ground. Fig. 3 shows the profile and instrumentations of test specimen under the similitude of 1/25 scaled model and the time history of the shaking table acceleration obtained for the shake event No. 5, at which the reinforcing bar of piles had yielded. Here, the test results obtained with the event No. 5 are shown in Fig. 6 together with the three-dimensional effective stress analysis results. The details of the centrifuge model and test results can be referred to [9] and [10]. The pile damage after the final event No. 6 is shown in Photo 1.

3.2 Method

In the analysis, “FINAL-GEO”, a large-scale high-speed nonlinear FEM analysis program was used [11]. In “FINAL-GEO”, in addition to the constitutive model of reinforced concrete, Biot's multi-dimensional consolidation of saturated porous media [12] and the effective stress analysis incorporating the constitutive model of soil in Chapter 2 are used. The seismic response of saturated ground and RC structures can be obtained in consideration of the generation and dissipation processes of excess pore-water pressure according to the during and the post-earthquake. Here, in the formulation of the finite element method for saturated ground, the *u-U* formulation using the absolute displacement of pore-water is adopted [13].

3.3 Model

Fig. 4 shows the analytical model which the symmetry in the shape and loading conditions concerned. Therefore, half in the width direction is modeled as shown in Fig. 3. Hexahedral elements are adopted for steel superstructures, footings and ground, truss elements are adopted for reinforcing bar and lateral bar of shear in pile foundation, and quadrilateral elements are adopted for footing steel mold. Relative slip between concrete and reinforcing bars is not modeled. The joint elements with a shearing stiffness of zero for the interface between the footing, pile and the liquefiable ground are installed considering the slip between each other. An infinite normal stiffness at the time of tensile stress action is assumed as well.

3.4 Boundary conditions

The model is completely fixed at the bottom boundary. Because of utilizing the shearing stack container, a subordinate condition is given so that the horizontal displacement of the nodes on both sides of the ground (displacement in the x direction in Fig. 4). The mass of the container is considered as concentrated mass and the stiffness is considered as a shear spring. The reproduction analysis was performed for the event No. 5 at which the yielding of reinforcing bar on the pile was observed. The recorded acceleration obtained at the bottom of the shearing stack container was used as the input motion.

3.5 Physical and mechanical properties

Table 2 shows the physical and mechanical properties of liquefiable ground. The relative density of 63% was prepared for the liquefiable ground in the test, the material constants for isotropic hardening/softening due to shear is set as μ=0. Elasticity was assumed as the supporting ground.

3.6 Reinforced concrete model

Fig. 5 shows the relationship between principal stress and equivalent uniaxial strain of concrete under monotonic loading. The Modified Ahmad model [14] was used for the ascending region, the Nakamura model [15] for the softening region in the compressive side and the coefficients at compressive failure in the Ottosen model [16] was used proposed by Hatanaka et al. The tensile side was assumed to be linear up to the cracking, and after the cracking was assumed to be softened [17]. The hysteresis characteristics under cyclic loading were expressed by Naganuma et al. The stress-strain relationship of the reinforcing bars was assumed to be a complete elasto-plastic model with the yield strength as the break point.

3.7 Results

Fig. 6 shows the time history of footing, ground surface acceleration and excess pore-water pressure ratio of saturated ground, footing displacement, and reinforcing bar of strain at pile head (tensile: positive, compression: negative). In saturated ground, the excess pore-water pressure ratio reaches about 1.0 in about 0.4s to 0.5s, and liquefaction occurs. After the liquefaction, the acceleration of the ground surface is attenuated, but the footing has a significant oscillation continuously. Its tendency is the same as the centrifuge model test. The excess pore-water pressure ratio in the analysis rises slightly faster than the test results, but the time to reach liquefaction is sufficiently reproduced. In the strain response of reinforcing bar, the footing displacement is positive (to the right in Fig. 3), the reinforcing bar of pile head B1-M1 is in compression and the reinforcing bar of pile head B1-M6 is in tension. Pile head strain of B1-M1 and B1-M6 were consistent with the phase characteristics of reinforcing bar. In the centrifuge test, a tensile strain of 3247μ was generated at pile head B1-M6, and the yield of the reinforcing bar was observed. However, a tensile strain of 918μ at pile head B1-M6 is observed in the analysis, which far from the yield of reinforcing bar. The footing displacement is also underestimated compared to the test results. This is possibly due to the insufficient reproductivity of liquefied soil response. Because of the shear strain of the ground near the failure is almost steady in the constitutive model of soil as shown in Fig. 2, the occurrence of a large shear strain is interfered in liquefied soil elements.

As for the damage of the piles in Photo 1, mainly bending cracks were observed, but no shear cracks occurred. From the comparison with the crack location observed after the centrifuge test, in both cases, bending cracks occurred at the pile head, pile end and pile middle, and there were no oblique cracks due to shear, and the qualitative tendency could be reproduced in the reproduction analysis.

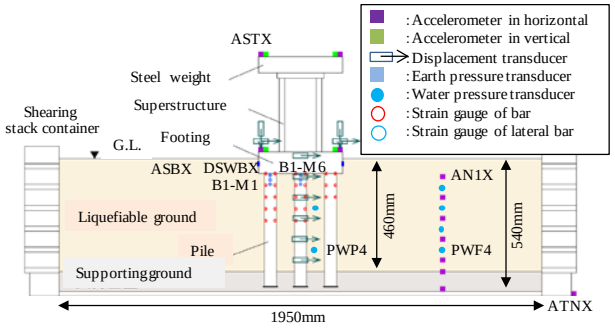

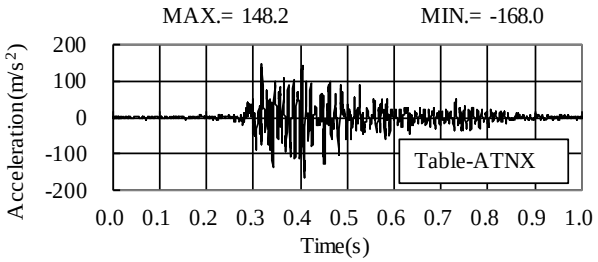

Fig. 3 Location of transducers and time history of acceleration at shaking table (Oscillation No. 5)

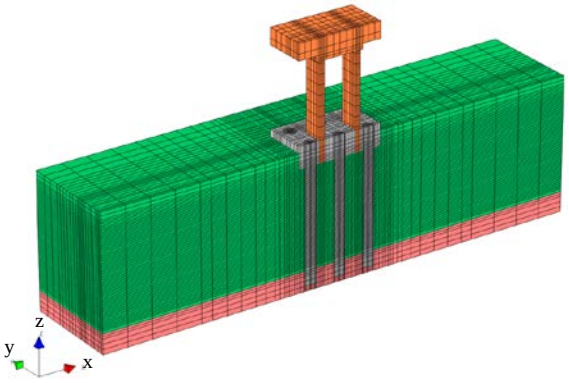

Fig. 4 Analytical model

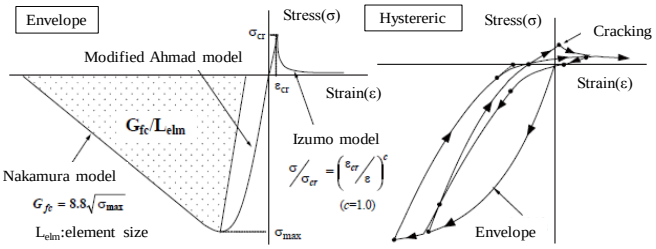

Fig. 5 Relationship between stress and strain for concrete

Table 2 Physical properties and mechanical properties

Material	Silica sand No. 7 (D_r=60%)	
Grain density	ρ_s	2.648t/m^3
Pore-fluid density	ρ_f	1.0t/m^3
Porosity	n	0.472
Grain bulk modulus	K_s	1.0×10^{40}kN/m^2
Pore-fluid bulk modulus	K_f	2.25×10^{6}kN/m^2
Permeability	k	7.0×10^{-5}m/s

(Centrifuge model test)

(Effective stress analysis)

Photo 1 Comparison of damage of pile foundation between centrifuge model test and effective stress analysis

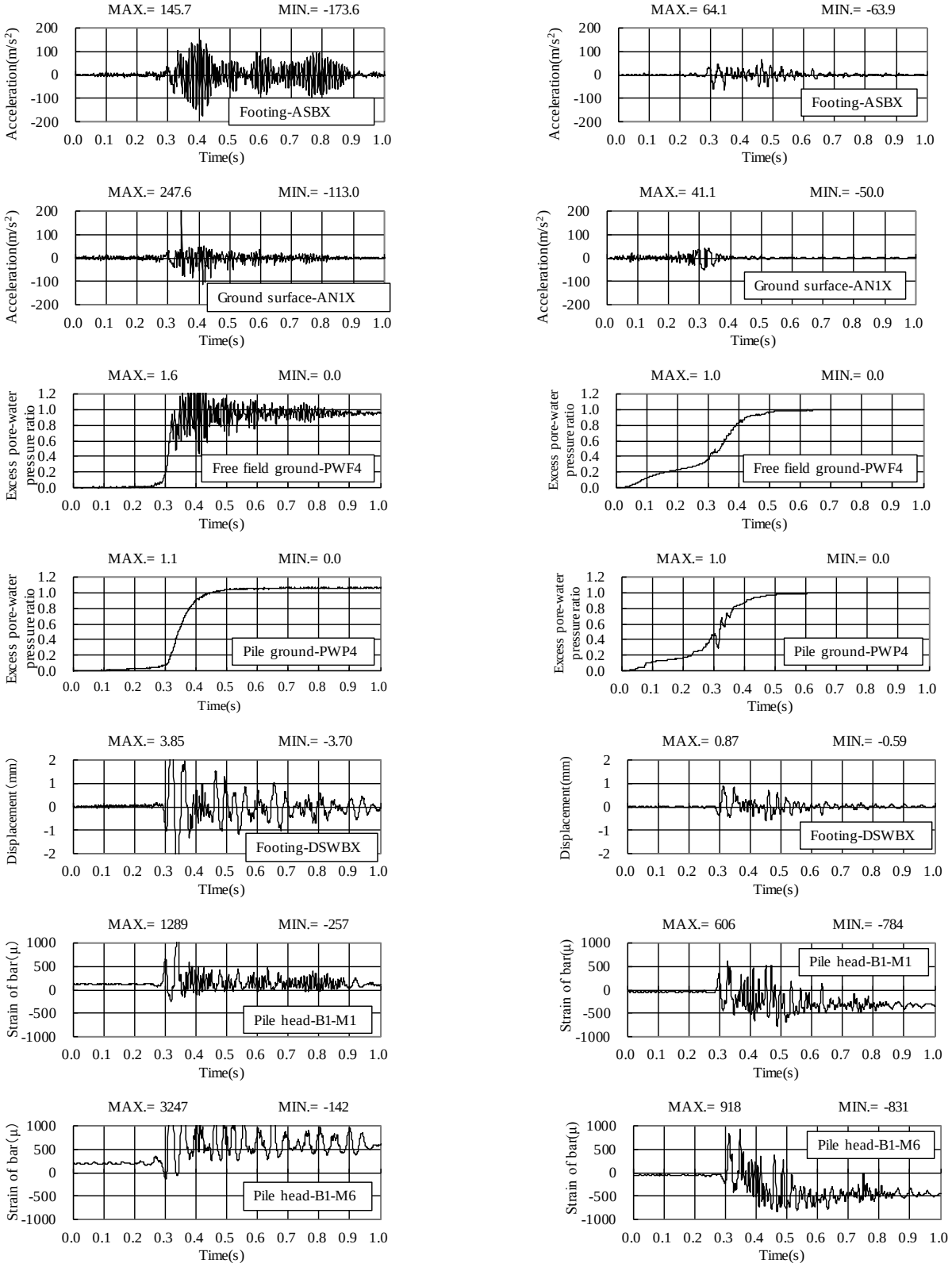

(Centrifuge model test) (Effective stress analysis)

Fig. 6 Comparison of time histories between centrifuge model test and effective stress analysis

4. 3D effective stress analysis of cement-treated soil improvement

4.1 Model

Fig. 7 shows profile of a target model (a representative case as replacement ratio of 50%), of which the countermeasure against liquefaction utilizing a lattice-type cement-treated soil improvement is implemented. As previously mentioned, this countermeasure is more economical than the block-type cement-treated soil improvement. The rational replacement ratio of the countermeasures for the underground RC structure in the liquefiable ground is examined as an example. The underground RC structure shown in Fig. 8 is designed in accordance with the open-cut railway tunnel standard [18]. The structural specifications are followings. (a) Design concrete strength of F_c=24N/mm^2, (b) Reinforcing bar of SD345, (c) The ratio of tensile reinforcing bar P_t is 1.13% (outside) and 1.59% (inside) on upper slab and side wall, (d) The ratio of tensile reinforcing bar P_t is 0.79% (both outside and inside) on bottom slab and center wall and (e)The ratio of shear reinforcing bar P_w is uniformly 0.25%, respectively. Table 3 shows the dimensions and specifications of the lattice-type cement-treated soil improvement body. Here, the aspect ratio of lattice is defined as the ratio of the unimproved ground length inside the lattice (=internal of lattice/height of improvement). Analytical cases are chosen as the unimproved case and cases with replacement ratio a_p of 40%, 50% and 60%. Fig. 9 shows a 3D profile of analytical model (a_p =50%). The depth of the model is same as one unit of the interval of lattice (same as width of improvement) including the unimproved ground inside the lattice. Fig.10 shows seismic motion, NS component of JMA Kobe wave as Level 2 earthquake motion with duration of 14s.

4.2 Physical and mechanical properties of liquefiable ground and cement-treated soil improvement body

In the liquefiable ground, D_r=60% (liquefaction strength ratio R_{20} of 0.2) is assumed, which is relatively weak, so the mechanical properties μ=0 and the physical properties in Table 1 and 2 are used as parameters for the subloading surface model. The supporting ground is assumed to be elastic (ρ_t=2.0t/m^3, V_s=700m/s). Table 4 shows mechanical properties of cement-treated soil improvement body. The initial value F_0 of the normal-yield surface and the tensile strength ratio ξ are chosen simultaneously satisfying the two points corresponding to the compressive strength σ_c of 2250kN/m^2 and tensile strength σ_t of 450kN/m^2, and the critical state lines on the compression side and extension side as M_c= 1.636 and M_t=1.059 on the p-q plane of the Modified cam-clay model. Therefore, this reflects the nonlinear behavior of stress and strain considering both compressive strength and tensile strength of the cement-treated soil improvement body precisely.

4.3 Reinforced concrete model

Concrete is a constitutive model similar to that of Section 3.6, but Ottosen's model [16] under the condition of compression failure, and the Naganuma model for shear transfer characteristics after cracking is used in this analysis. Details of the constitutive model can be provided in Ref. [14]. Reinforcing bars are modeled as embedded reinforcing bars, which added the rigidity of concrete elements with the rigidity equivalent to that of reinforcing bars. The constitutive model of the reinforcing bars is the bilinear model with the yield strength as the break point, the stiffness after exceeding the yield point is 1/100 of the initial stiffness. The material model and constants of the structure are the same as in Ref. [18].

4.4 Results

Fig. 11 shows the time history of the excess pore-water pressure ratio at the center of unimproved ground, inside the lattice of the left and right lattice-type cement-treated soil improvement (G.L.-7.75m). The time history obtained in liquefiable ground at free field is also shown. It is pointed out that, as the replacement ratio increases, the same as the aspect ratio of lattice decreases, the excess pore-water pressure ratio of the unimproved ground inside the lattice gradually becomes smaller than that of the free field.

Fig. 12 (a) shows the time history of the relative displacement, which defined as the difference between the top and bottom slab, of the center wall at the middle depth of the structure according to the replacement ratio including unimprovement case. The reinforcing effect corresponding to the replacement ratio is obtained by normalizing the displacement of the unimprovement case in Fig.12 (b), as well. Here, regarding with the replacement ratio, the interval of lattice (width of improvement) is different for each of 40%, 50% and 60%.

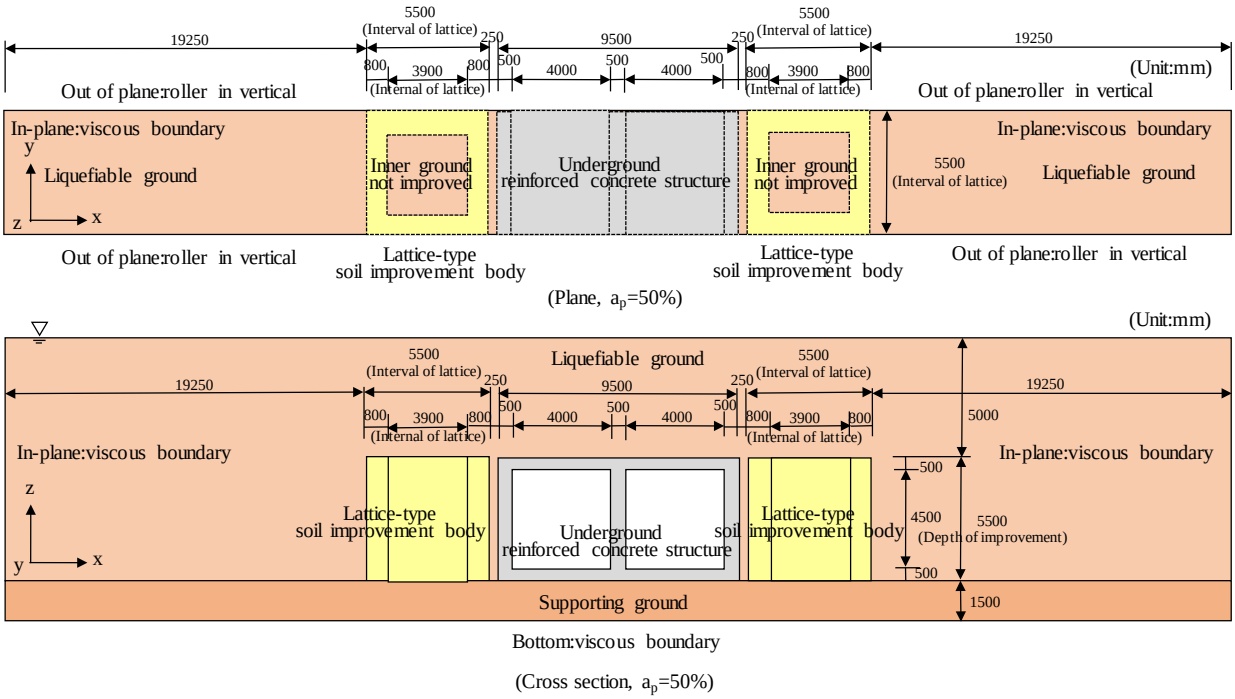

Fig. 7 Target model (Lattice-type cement-treated soil improvement, replacement ratio of 50%)

Table 3 Dimension and specification for lattice-type cement-treated soil improvement body

Replacement ratio a_p	Interval of lattice (width of improvement)	Internal of lattice	Aspect ratio of lattice	Equivalent replacement ratio a_p'
Unimproved	—	—	—	—
40%	7.1m	5.5m	1.00	67%
50%	5.5m	3.9m	0.71	50%
60%	4.35m	2.75m	0.50	38%
Remarks	Thickness of wall：0.8m Height of improvement：5.5m			

Table 4 Mechanical properties (cement-treated soil improvement)

Compressional index	ρ, $\lambda/(1+e_0)$	0.31125
Swelling index	γ, $\kappa/(1+e_0)$	0.01085
Internal frictional angle	ϕ_f	40°
Initial normal-yield surface	F_0	2927kN/m^2
Poisson's ratio	ν	0.167
Limit surface of rotational hardening	ϕ_b	0
Evolution of rotational hardening	b_r	0
Evolution of normal-yield subloading surface size ratio R	u	5000
	ζ_1	0
Ratio related to initial normal-yield surface	ξ	0.0728
Elastic modulus	E_0	3500000kN/m^2

$$a_p' = \frac{(\text{Interval of lattice})^2}{(5.5m)^2} \times a_p \quad (4)$$

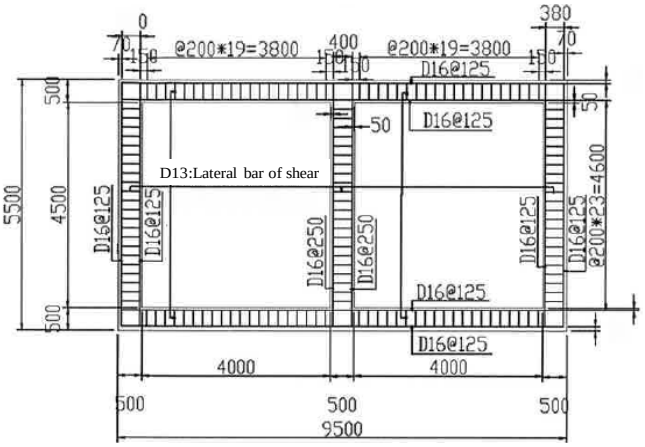

Fig. 8 Specification for underground RC structure

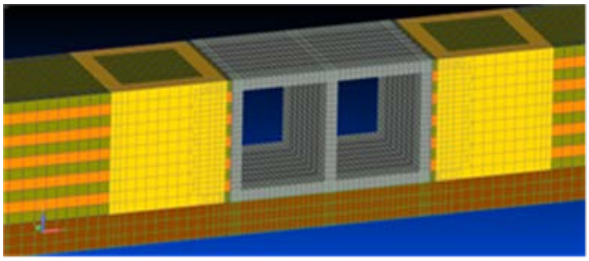

Fig. 9 Analytical model (replacement ratio of 50%)

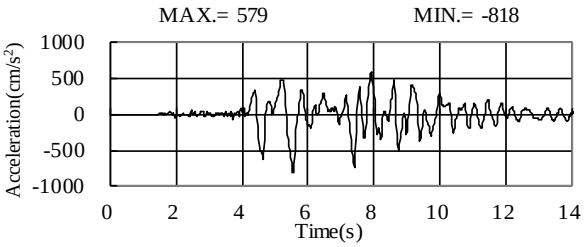

Fig. 10 Time history of earthquake motion

Therefore, the equivalent replacement ratio a_p' is newly defined normalized by the interval of lattice at replacement ratio a_p=50% of 5.5m as obtained by Eq. (4). Table 3 shows the equivalent improvement ratio a_p' together with improvement ratio a_p. In case of the unimproved case, the deformation angle of the center wall of the RC structure is 1.56%. Because of the reduction in relative displacement on the side wall and center wall of underground structures, as the replacement ratio increased, the deformation angle of the center wall is reduced to 0.19% at replacement ratio of 50%.

Fig. 13 shows distributions of deformation and reinforcing bar strain of the structure for soil unimproved case at t=5.75s. Distributions of the octahedral shear stress and octahedral shear strain of the cement-treated soil improvement body with a replacement ratio a_p' =50% at t=5.65s are shown in Fig. 14. For unimproved case, the maximum bar strain of 0.66% in the x-direction, and that of 1.03% in the z-direction are analyzed. In case of the replacement ratio a_p' =38%, the bar of strain is 0.10% in the x-direction and 0.21% in the z-direction. The shear stress and shear strain at the bottom corner of the cement-treated soil improvement body are 1252kN/m^2 and 0.21%, which exceed the yield stress and strain. On the other hand, at replacement ratio a_p' =50%, bar yield is suppressed as well as the shear stress at the bottom corner of the soil improvement body with regard to the yield limit. Therefore, the economical replacement ratio of about a_p = 50% can be confirmed to be appropriate for the lattice-type soil improvement in this example.

5. Summary

As a nonlinear analysis method for RC structures in liquefiable ground, a three-dimensional effective stress analysis method is developed incorporating an extended constitutive model for a wide range of saturated sand that expresses the generation, accumulation and dissipation of excess pore-water pressure during and post-earthquake. The following summarizes the findings obtained in this study.

1) Conducting the three-dimensional effective stress analysis method to the reproduction analysis of the centrifuge model test of RC pile foundations in liquefiable ground, the response of structures, liquefiable ground and RC piles tends to be qualitative in test and analysis and was confirmed that the coupled nonlinear behavior of the liquefiable ground and the RC structure can be reproduced.

2) On the lattice-type cement-treated soil improvement as countermeasure against liquefaction, based on the 3D effective stress analysis, underground RC structure with a soil improvement width equivalent to the height of is structure and a replacement ratio of 50% was shown to be secured during strong earthquake.

3) In the seismic design for countermeasure against liquefaction by the lattice-type cement-treated soil improvement, if the 3D effective stress analysis method is applied, it is expected to be a reasonably improved specification compared to the conventional 2D effective stress analysis.

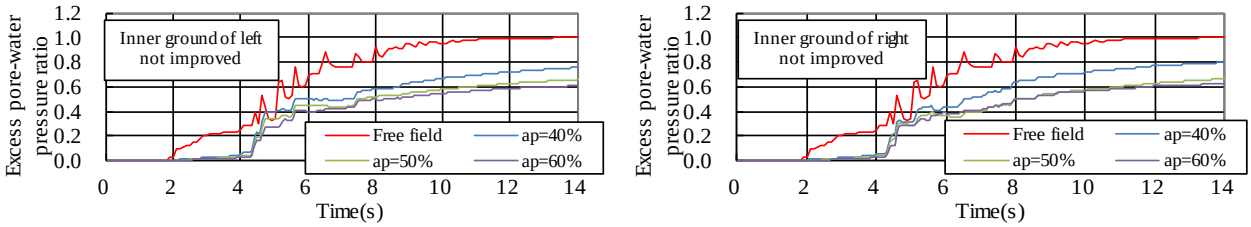

Fig. 11 Excess pore-water pressure ratio at liquefiable ground surrounded with lattice-type soil improvement

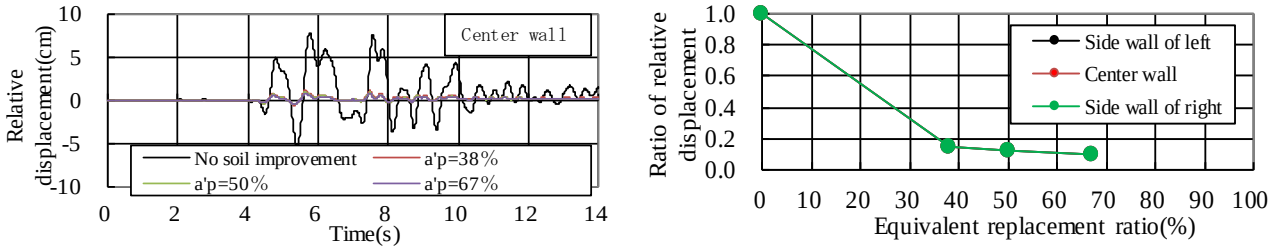

Fig. 12 (a)Relative displacement at RC structure (b)reinforcing effect according to equivalent replacement ratio

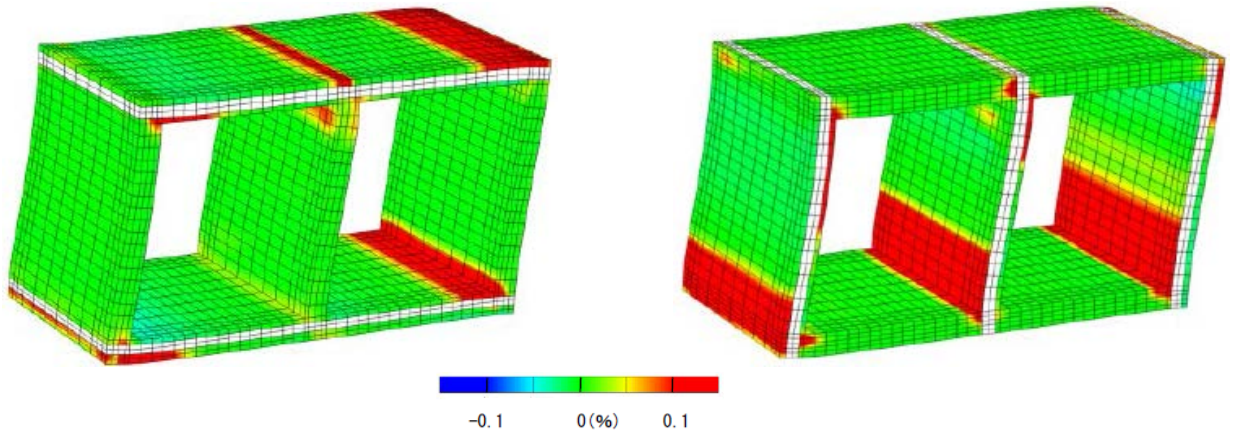

Bar of x-direction in horizontal, dispalcement scale of 10 times

Bar of z-direction in vertical, displacement scale of 10 times

Fig. 13 Deformation of structure and strain of reinforcing bars (no cement-treated soil improvement)

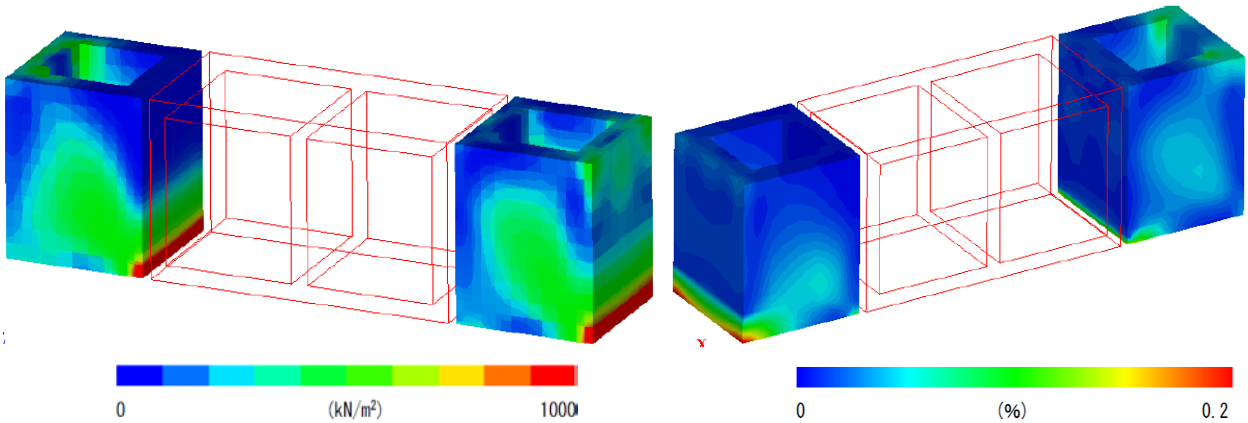

Fig. 14 Octahedral shear stress and Octahedral shear strain of soil improvement body (cement-treated soil improvement available, replacement ratio of 50%)

6. References

[1] Kazuhiko Urano, Atsushi Nishimura, Yuji Adachi, Makoto Kawamura (2012.2): Horizontal loading test on seismic reinforcement of underground structures using ground improvement bodies, Report of Hazama Research Institute.

[2] Hiroshi Furuya, Kiyoshi Sato, Takashi Matsuda (1999): Analytical examination of lattice-shaped ground improvement as a liquefaction countermeasure construction method, 25th Earthquake Engineering Research Conference, Japan Society of Civil Engineers, pp. 397-400 (in Japanese).

[3] Ryosuke Uzuoka, Noriaki Sento, Atsushi Yashima, Zhang Xiao (2002): Three-dimensional effective stress analysis of pile foundation structures located near the revetment, Japan Earthquake Engineering, Vol. 2, No. 2, pp. 1-14 (in Japanese).

[4] Namikawa, T., Koseki, J. and Suzuki, Y. (2007): Finite element analysis of lattice shaped ground improvement by cement-mixing for liquefaction mitigation, Soils and Foundations, Vol. 47, No. 3, pp. 559-576.

[5] Koichi Hashiguchi (1995): Latest Elastoplasticity, pp.155-161, Asakura Shoten (in Japanese).

[6] Hashiguchi, K. and Chen, Z.-P. (1998): Elastoplastic constitutive equation of soils with the subloading surface and the rotational hardening, Int. J. for numerical and analytical methods in geomechanics, Vol. 22, pp. 197-227.

[7] Hashiguchi, K. and Mase, T. (2007): Extended yield condition of soils with tensile yield strength and rotational hardening, Int. J. of plasticity 23, pp. 1939-1956.

[8] Koichi Hashiguchi, Shinya Mase (2010): Physical interpretation and quantitative expression of cyclic mobility by subloading surface model, Geotechnical Journal, Vol. 6, No. 2, pp. 225-241 (in Japanese).

[9] Shunichi Higuchi, Takahiro Tsutsumiuchi, Rinna Otsuka, Koji Ito, Joji Ejiri (2012): Centrifugal model vibration test of RC pile foundation, Proceedings of JSCE A1 (Structure and Earthquake Engineering), Vol. 68, No. 4 (Earthquake Engineering Papers Vol.31-b), pp. I_642-I_651 (in Japanese).

[10] Kenji Yonezawa, Takuya Anabuki, Shunichi Higuchi, Koji Ito, Takahiro Tsutsumiuchi, Joji Ejiri: Seismic response FEM analysis of ground-structure coupled system using three-dimensional large-degree-of-freedom model, Bulletin of Obayashi Institute of Technology, No. 76, 2012.12 (in Japanese).

[11] Yonezawa Kenji, Anabuki Takuya, Ejiri Joji (2011): Large-scale, high-speed nonlinear FEM analysis software "FINAL-GEO", Obayashi Institute of Technology Research Report, No. 75 (in Japanese).

[12] Biot, M. A. (1941): General theory of three-dimensional consolidation, J. Appl. Phys., Vol. 12, pp. 155-164.

[13] Zienkiewicz, O. C. and Shiomi, T. (1984): Dynamic behavior of saturated porous media; the generalized Biot formulation and its numerical solution, Proc. of Int. J. for Numerical and Analytical Methods in Geomechanics, Vol. 8, pp. 71- 96.

[14] Naganuma, K., Yonezawa, K., Kurimoto, O. and Eto, H . (2004): Simulation of nonlinear dynamic response of reinforced concrete scaled model using three-dimensional finite element method, 13th WCEE, Vancouver, BC, Canada, Paper No. 586.

[15] Nakamura, H. and Higai, T. (1999): Compressive fracture energy and fracture zone length of concrete, Seminar on Post-peak Behavior of RC Structures Subjected to Seismic Load, JCI-C51E, Vol. 2, pp. 259-272.

[16] Kazuhiro Naganuma (1995): Stress-strain relationship of concrete under triaxial compression, Architectural Institute of Japan, 474, pp. 163-170 (in Japanese).

[17] Izumo Shinichi, Shima Hiroshi, Okamura Minoru (1987): Analytical model of reinforced concrete plate elements subjected to in-plane force, Concrete engineering, Vol. 25, No. 9, pp. 107-120 (in Japanese).

[18] Tomohiro Sasaki, Shunichi Higuchi (2017): Study on damage mechanism of box culvert subjected to fault displacement, Journal of Japan Society of Civil Engineers A1 (Structure and Earthquake Engineering), Vol. 74, No. 4 (Volume 37 of Earthquake Engineering), pp. I_395-I_406 (in Japanese).

